

Oscillations and Bifurcation Structure of Reaction-Diffusion Model for Cell Polarity Formation

Masataka Kuwamura^{*}, Hirofumi Izuhara[†] and Shin-ichiro Ei[‡]

Abstract

We investigate the oscillatory dynamics and bifurcation structure of a reaction-diffusion model for cell polarity formation in [Otsuji et al, PLoS Comp. Biol. 3 (2007), e108]. We show that this model can represent formation processes from a homogeneous initial cell to a polarized cell. The polarized cells can be classified into three types including the type of cell polarity oscillations. In particular, it is shown that the Turing instability can be a trigger which eventually leads to cell polarity oscillations with the reversal of polarity as observed in bacteria cells and melanoma cells. Moreover, we investigate the effect of extracellular signaling on cell polarity oscillations.

Keywords: cell polarity oscillations, reaction-diffusion system

Running head: Oscillations and Bifurcation Structure

Mathematics subject classification: 35K57, 92B05

Corresponding author: Masataka KUWAMURA

^{*}Graduate School of Human Development and Environment, Kobe University, Kobe 657-8501, Japan, email: kuwamura@main.h.kobe-u.ac.jp

[†]Faculty of Engineering, University of Miyazaki, 1-1 Gakuen Kibanadai-nishi, Miyazaki, 889-2192, Japan, email: izuhara@cc.miyazaki-u.ac.jp

[‡]Department of Mathematics, Hokkaido University, Sapporo 060-0810, Japan, email: Eichiro@math.sci.hokudai.ac.jp

1 Introduction

Cells in an epithelial tissue are organized into layers. The functionality and form of the layer depends on the coordinated polarization of each cell. The maintenance of cell polarity in a developing epithelial tissue is a dynamic process with an alternating repetition of the establishment and loss of polarity in a cell cycle-dependent manner. This repetition is a typical example of cell polarity oscillations [3], where the reversal of polarity does not occur.

Cell polarity oscillations are also observed in cell migration which is the directed movement of a single cell or a group of cells in response to chemical and/or mechanical signals. For example, bacteria cells during rippling (the accordion-like movements) [4, 18], migrating melanoma cells derived from tumors [16], can reverse their polarity in an oscillatory fashion. Although the detailed molecular mechanisms underlying cell polarity oscillations in various examples are different, they often incorporate with conserved G-proteins based signaling systems which are commonly observed from bacterial to mammalian cells. Therefore, we expect a simple and universal principle for understanding cell polarity oscillations.

For understanding cell polarity oscillations, some mathematical models have been proposed. For example, [16] proposed an ODE system based on biomolecular dynamics at the front and back lamellipodia in a migration cell to understand their experimental results about changing of cell polarity in melanoma cells derived from tumors. [4] proposed an ODE system based on three proteins to understand cell polarity oscillations with the polarity reversal of bacteria cells during rippling (the accordion-like movements) [18]. Recently, [19] generalized the ODE system in [4], and proposed an ODE system which gives four different mechanisms for switching cell polarity, including a mechanism to generate the periodic reversal of polarity. [11] proposed

a delay reaction-diffusion equation with nonlocal term for studying the effects of delayed negative feedback on cell polarity oscillations with the aid of numerical simulations.

In this paper, we consider a reaction-diffusion model for cell polarity formation proposed by [15]

$$\begin{cases} \dot{u} &= d_1 u_{xx} - f(u, v) \\ \dot{v} &= d_2 v_{xx} + f(u, v), \end{cases} \quad (1.1)$$

where

$$f(u, v) = -a_1(u + v)\{(\alpha u + v)(u + v) - a_2\} \quad (1.2)$$

with

$$\alpha = \frac{d_1}{d_2},$$

and d_1, d_2, a_1 and a_2 are positive constants. Here, u and v stand for concentrations of two internal chemicals in a cell; u and v correspond to chemicals in the membrane and cytosol, respectively. Since the diffusion in cytosol is faster than that in the membrane, the diffusion coefficients d_1 and d_2 satisfy the condition

$$d_1 < d_2,$$

which implies $0 < \alpha < 1$. Moreover, by setting $a_2 \rightarrow a_2 - \varepsilon a_E(x)$ in (1.2), we obtain a perturbed system of (1.1), i.e.,

$$\begin{cases} \dot{u} &= d_1 u_{xx} - \{f(u, v) - \varepsilon g(x, u, v)\} \\ \dot{v} &= d_2 v_{xx} + \{f(u, v) - \varepsilon g(x, u, v)\} \end{cases} \quad (1.3)$$

with

$$g(x, u, v) = a_1(u + v)a_E(x), \quad (1.4)$$

where $a_E(x)$ is a smooth function which represents the waveform of an extracellular signaling, and ε is a small positive parameter which controls the

amplitude of the extracellular signaling. We consider (1.1) and (1.3) on an interval $I = (-K/2, K/2)$ under the periodic boundary condition for sufficiently large K .

In general, a reaction-diffusion system (1.1) with a smooth function f is called a reaction-diffusion system with mass conservation because

$$\int_0^L (u(x, t) + v(x, t)) dx \equiv \int_0^L (u(x, 0) + v(x, 0)) dx \quad (1.5)$$

holds for any (smooth) solutions under the periodic or Neumann boundary conditions. For certain functions f and boundary conditions, some mathematical aspects of (1.1) have been studied in [5, 7, 12, 13], and one of the typical dynamics of (1.1) is summarized as follows: solutions with initial values near a homogeneous equilibrium destabilized through the same mechanism as Turing instability eventually approach a localized unimodal stationary pattern (See, Fig. 1). This dynamics is interpreted as cell polarization, and the position of the peak of the localized unimodal pattern determines the direction of polarity. As for the function f given by (1.2), it was numerically shown in [15] that (1.1) has such dynamics under certain conditions. In addition, [15] performed a formal stability analysis for the final localized unimodal stationary pattern of (1.1), and numerically showed that a solution of (1.3) starting from the final pattern of (1.1) can translationally move to the maximum point of $a_E(x)$ when $a_E(x)$ is given by $a_E(x) = A \cos(2\pi x/K)$. This implies that cell polarity can be controlled by extracellular signaling.

On the other hand, by using the normal form theory, it was shown in [14] that (1.1) can have a unimodal stationary pattern which changes its stability due to a Hopf bifurcation when we vary d_1 as a bifurcation parameter. Consequently, (1.1) with (1.2) has a spatially nonhomogeneous limit cycle with small amplitude under certain conditions.

The purpose of this paper is to show that (1.1) with (1.2) can represent formation processes from a homogeneous cell to a polarized cell. The polarized cells can be classified into three types including the type of cell polarity oscillations. We show that (1.1) with (1.2) has limit cycles with large amplitude by using numerical simulations (See, Fig. 2). These limit cycles exhibit an alternating repetition of unimodal patterns and spatially homogeneous patterns, and hence they can be interpreted as cell polarity oscillations. Moreover, by using numerical bifurcation analysis, we investigate the bifurcation structure of (1.1) with (1.2) which generates the limit cycles when we vary d_1 as a bifurcation parameter. Furthermore, when $a_E(x)$ is given by $a_E(x) = A \cos(2\pi x/K)$, we investigate the dynamics of (1.3) with (1.2) and (1.4). In particular, we numerically show that (1.3) with (1.2) and (1.4) has limit cycles exhibiting such an alternating repetition, and examine the position of the peak of the unimodal patterns periodically appearing to understand the controllability of cell polarity oscillations by extracellular signaling.

The remainder of this paper is organized as follows. In Section 2, we investigate spatiotemporal patterns of the unperturbed system (1.1) with (1.2). We give a concrete expression of a localized unimodal stationary pattern of (1.1) with (1.2) for sufficiently large K . It is a prominent feature that this model enables us to perform concrete calculations for mathematical analysis. Moreover, we numerically show the formation process of the localized unimodal stationary pattern and the existence of limit cycles which exhibit an alternating repetition of unimodal patterns and spatially homogeneous patterns. In particular, it is numerically shown that (1.1) with (1.2) has a solution which can be regarded as a formation process from a homogeneous cell to a polarized cell exhibiting cell polarity oscillations with the reversal

of polarity as observed in bacteria cells [4, 18] and melanoma cells [16]. In Section 3, by using numerical bifurcation analysis, we investigate the bifurcation structure of (1.1) with (1.2) when we vary d_1 as a bifurcation parameter. Our numerical bifurcation analysis shows that the limit cycles exhibiting the alternating repetition bifurcate from the localized unimodal stationary pattern through a Hopf bifurcation, and that the limit cycles become unstable through a period doubling bifurcation. These results support the results obtained by numerical simulations in Section 2, and enable us to understand that the Turing instability can be a trigger which eventually leads to cell polarity oscillations with the reversal of polarity. In Section 4, we investigate the dynamics of spatiotemporal patterns in the perturbed system (1.3) with (1.2) and (1.4) when $a_E(x)$ is given by $a_E(x) = A \cos(2\pi x/K)$. We analytically derive the equation of motion for the translational movement of the localized unimodal pattern, which gives a mathematical justification of the results in [15]. Moreover, we show that (1.3) with (1.2) and (1.4) has limit cycles exhibiting such an alternating repetition, and examine whether or not the position of the peak of the unimodal patterns periodically appearing can be determined by the maximum point of $a_E(x)$. These results are useful for understanding the effect of extracellular signaling on cell polarity oscillations. Concluding remarks are presented in Section 5.

2 Spatiotemporal patterns of unperturbed system

In this section, we investigate spatiotemporal patterns of the unperturbed system (1.1) with (1.2), which is useful for understanding spontaneous cell polarization without extracellular signaling. In particular, we numerically show limit cycles which exhibit an alternating repetition of unimodal patterns

and spatially homogeneous patterns. These limit cycles can be interpreted as cell polarity oscillations.

2.1 Concrete expression of localized unimodal stationary pattern

We give a concrete expression of a localized unimodal stationary pattern of (1.1) with (1.2) for sufficiently large K .

We consider stationary solutions of (1.1), i.e.,

$$\begin{cases} d_1 u_{xx} - f(u, v) = 0 \\ d_2 v_{xx} + f(u, v) = 0, \end{cases} \quad (2.1)$$

where $f(u, v)$ is given by (1.2). Applying a transformation of variables

$$p := u + v \quad \text{and} \quad q := \alpha u + v \quad (2.2)$$

to (2.1), we have

$$\begin{cases} q_{xx} = 0 \\ d_1 d_2 p_{xx} + (d_2 - d_1) a_1 p (pq - a_2) = 0. \end{cases} \quad (2.3)$$

Since q satisfies the periodic boundary condition, it follows from the first equation of (2.3) that $q(x) \equiv q_0$. Therefore, by the second equation of (2.3), we have

$$p_{xx} + c_1 p (p - c_2) = 0, \quad (2.4)$$

where

$$c_1 = \frac{(d_2 - d_1) a_1 q_0}{d_1 d_2} \quad \text{and} \quad c_2 = \frac{a_2}{q_0}.$$

On the other hand, direct calculation shows that

$$p(x) = p_0 \operatorname{sech}^2(bx)$$

satisfies (2.4) for

$$p_0 = \frac{3a_2}{2q_0} \quad \text{and} \quad b = \frac{1}{2} \sqrt{\frac{(d_2 - d_1)a_1a_2}{d_1d_2}}. \quad (2.5)$$

Therefore, noting (2.2), we see that

$$u = \varphi_1(x) := \frac{1}{d_2 - d_1} \left(d_2 p_0 \operatorname{sech}^2(bx) - \frac{3a_2 d_2}{2p_0} \right)$$

and

$$v = \varphi_2(x) := \frac{1}{d_2 - d_1} \left(-d_1 p_0 \operatorname{sech}^2(bx) + \frac{3a_2 d_2}{2p_0} \right)$$

satisfy (2.1). Since $\operatorname{sech}(bx) = O(e^{-b|x|})$ as $|x| \rightarrow \infty$, it is easy to see that (1.1) has a stationary solution $(\bar{u}(x), \bar{v}(x))$ satisfying the periodic boundary condition at $x = \pm K/2$, where

$$\bar{u}(x) = \varphi_1(x) + O(e^{-bK}) \quad (2.6)$$

and

$$\bar{v}(x) = \varphi_2(x) + O(e^{-bK}) \quad (2.7)$$

as $K \rightarrow \infty$. We consider that $(\bar{u}(x), \bar{v}(x))$ is a localized unimodal stationary pattern as shown in Fig. 1(b) when K is sufficiently large. Moreover, we note that $(\bar{u}(x - c), \bar{v}(x - c))$ for some $c \in [-K/2, K/2)$ is also a stationary solution of (1.1) because of the periodic boundary condition.

It follows from (2.6) and (2.7) that

$$\bar{u}(x) + \bar{v}(x) = p_0 \operatorname{sech}^2(bx) + O(e^{-bK}) \quad (2.8)$$

and

$$\alpha \bar{u}(x) + \bar{v}(x) = q_0 + O(e^{-bK}). \quad (2.9)$$

Since

$$\int_I \operatorname{sech}^2(bx) dx = \int_{-\infty}^{\infty} \operatorname{sech}^2(bx) dx + O(e^{-bK}) = \frac{2}{b} + O(e^{-bK}),$$

integrating (2.8) over $I = (-K/2, K/2)$, we have

$$p_0 = \frac{b}{2} \int_I (\bar{u}(x) + \bar{v}(x)) dx + O(K e^{-bK}) \quad (2.10)$$

as $K \rightarrow \infty$. This implies that the amplitude of the localized stationary pattern given by (2.6) and (2.7) can be explicitly determined by the total mass of components.

2.2 Formation of localized unimodal pattern

We numerically investigate the formation process of a localized unimodal pattern of (1.1) with (1.2). Our numerical simulations show that solutions starting from a spatially homogeneous initial state with small disturbance converge to $(\bar{u}(x - c), \bar{v}(x - c))$ for some $c \in [-K/2, K/2)$ under certain conditions, where \bar{u} and \bar{v} are given by (2.6) and (2.7), respectively.

Noting the mass conservation property (1.5) and (2.10), we see that the amplitude of the localized stationary solution given by (2.6) and (2.7) is determined by

$$p_0 = \frac{bK}{2} \xi \quad (2.11)$$

for sufficiently large K , where

$$\xi = \frac{1}{K} \int_I (u(x, 0) + v(x, 0)) dx \quad (2.12)$$

can be considered as a parameter. For each fixed ξ , we numerically solve (1.1) for various values of d_1 under the parameter values

$$a_1 = 0.5, \quad a_2 = 2.2, \quad d_2 = 1.0. \quad (2.13)$$

We choose $K = 10.0$ in such a way that $(\varphi_1(x), \varphi_2(x))$ can be numerically regarded as a stationary solution satisfying the periodic boundary condition. The initial value $(u(x, 0), v(x, 0))$ is given by $(\xi/2, \xi/2)$ with a small random

perturbation. Notice that these parameter values are the same as those in [15].

We use a numerical scheme in [10] based on the pseudospectral method; we obtain numerical solutions of (1.1) on $0 \leq x \leq K$, which can be regarded as those on $-K/2 \leq x \leq K/2$ under the periodic boundary condition. Fig. 1 shows that numerical solutions converge to the localized unimodal stationary pattern given by $(\bar{u}(x - c), \bar{v}(x - c))$ for some $c \in [-K/2, K/2)$ under the parameter value (2.13) for $d_1 = 0.1$ when $\xi = 2.0$. Notice that we cannot predict the value of c , the position of the peak of the localized unimodal stationary pattern, because of a small random perturbation to the initial value of solutions. The formation process of a localized unimodal stationary pattern as presented in Fig. 1 can be interpreted as cell polarization [15].

Our simulations show that when $\xi = 2.0$, numerical solutions converge to a (localized) unimodal stationary pattern for $d_1 \lesssim 0.73$, where the accuracy of approximation for the (localized) unimodal pattern by $(\bar{u}(x - c), \bar{v}(x - c))$ becomes lower as d_1 increases. We can obtain similar results when $\xi \gtrsim 0.68$.

Remark 2.1 The numerical simulations for large values of ξ are delicate task. In fact, when $\xi = 2.0$, the numerical result shown in Fig. 1 can be obtained if we adopt the time step as $\Delta t = 0.02$. In contrast, when $\xi = 6.0$, we can obtain a correct numerical result as shown in Fig. 1 if $\Delta t = 0.01$.

2.3 Spatiotemporal oscillatory patterns

We cannot observe that numerical solutions converge to the localized unimodal stationary pattern given by $(\bar{u}(x - c), \bar{v}(x - c))$ under certain conditions. In fact, when $\xi \lesssim 0.66$, our simulations show that the localized unimodal stationary pattern becomes unstable and spatiotemporal oscillatory patterns appear for some values of d_1 under the parameter values (2.13).

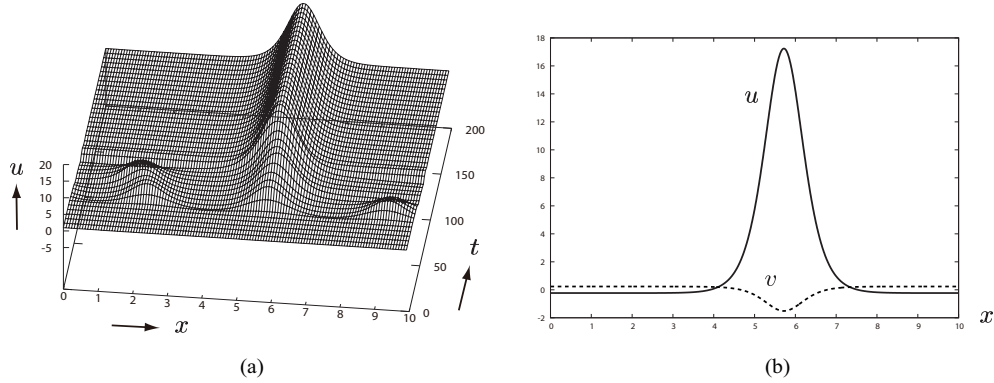


Figure 1: Formation of a localized unimodal stationary pattern for $d_1 = 0.1$ when $\xi = 2.0$. The initial value $(u(x, 0), v(x, 0))$ is given by $(\xi/2, \xi/2)$ with a small random perturbation. (a) The dynamics of u -component. The values of $u(x, t)$ on $0 \leq x \leq 10$ and $0 \leq t \leq 200$ are represented by a 3D graph. The profile of $v(x, t)$ is omitted here because the amplitude and spatial variation of $v(x, t)$ for each t are relatively small compared to those of $u(x, t)$. (b) The profiles of $u(x, t)$ and $v(x, t)$ for $t = 200$, which can be regarded as the localized unimodal stationary pattern given by $(\bar{u}(x - c), \bar{v}(x - c))$ for some $c \in [-K/2, K/2)$. The rigid and dashed lines represent u - and v -components, respectively. The numerical solutions on $0 \leq x \leq 10$ presented in this figure can be regarded as those on $-5 \leq x \leq 5$ under the periodic boundary condition. It should be noted that we cannot predict the value of c , the position of the peak of the localized unimodal pattern in u -component, because of a small random perturbation to the initial value.

In the same way as the previous subsection, we perform numerical simulations for $d_1 = 0.1, 0.25, 0.4$ and $d_1 = 0.8$ when $\xi = 0.6$. Fig. 2 shows that various spatiotemporal patterns appear when $\xi = 0.6$. Fig. 2 (a) shows a localized unimodal stationary pattern which can be interpreted as the persistent maintenance of cell polarity. Fig. 2 (b) and (c) show stable limit cycles with large amplitude, which exhibit an alternating repetition of unimodal patterns and spatially homogeneous patterns. Fig. 2 (c) shows that the localized unimodal patterns periodically appearing take their maximum at $x = x_0$ for some $x_0 \in [-K/2, K/2]$ when $d_1 = 0.4$. In contrast, Fig. 2 (b) shows that the localized unimodal patterns periodically appearing take their maximum at $x = x_1$ or $x = x_2$ alternatively for some $x_1 \in [-K/2, K/2]$ and $x_2 \in [-K/2, K/2]$ with $|x_2 - x_1| \approx K/2$ when $d_1 = 0.25$. These limit cycles in Fig. 2 (b) and (c) can be interpreted as cell polarity oscillations. The limit cycle in Fig. 2 (c) represents cell polarity oscillations with no reversal of polarity. On the other hand, noting that x_2 is antipodal to x_1 , the limit cycle in Fig. 2 (b) represents cell polarity oscillations with the reversal of polarity. We cannot predict the position of the peak of the localized unimodal patterns in Fig. 2 (a)–(c) because of a small random perturbation to the initial value. Fig. 2 (d) shows a spatially homogeneous stationary pattern which can be interpreted as nonpolarized cells.

Remark 2.2 In the case of melanoma cells [16, Figure 2], spatially homogeneous stationary patterns as in Fig. 2 (d) may be considered as cells which randomly polarize into frequently changing directions.

The numerical results in this section show that (1.1) with (1.2) has a solution which can be regarded as a formation process from a homogeneous initial cell to a polarized cell exhibiting cell polarity oscillations. Noting (1.5) and (2.12), we can observe cell polarity oscillations when the spatial average

of the sum of two internal chemicals in a cell is relatively small. In the next section, we investigate the bifurcation structure of (1.1) with (1.2) generating the dynamics shown in our numerical simulations.

3 Numerical bifurcation analysis

In this section, we numerically demonstrate that the bifurcation diagram of (1.1) with (1.2) contains a structure which generates spatiotemporal patterns presented in the last section. By using AUTO [2], a software package used for studying the bifurcation structure of ODE systems, we investigate the bifurcation diagram of an ODE system that is obtained by the finite Fourier series approximation for (1.1) with (1.2) in the same way as [8]. We investigate the bifurcation diagram of the ODE system with respect to d_1 for some fixed values of ξ under the parameter values (2.13) and $K = 10.0$.

Fig. 3 shows the bifurcation diagram for $\xi = 1.0$. The primary branch starting from $d_1 = 0.8$ represents a family of spatially homogeneous equilibria $(u(x), v(x)) = (\frac{a_2 - \xi^2}{(\alpha - 1)\xi}, \frac{\alpha\xi^2 - a_2}{(\alpha - 1)\xi})$ with $\alpha = d_1/d_2$. By using the standard linear stability analysis, we can easily verify that these equilibria are stable for $0.74 \lesssim d_1 \leq 0.8$ whereas unstable for $0 < d_1 \lesssim 0.74$. Moreover, it is easy to see that $d_1 \approx 0.74$ is characterized by $\text{Re}\lambda_1 = 0$, where λ_1 is the eigenvalue associated to the Fourier mode $e^{2\pi x/K}$. The secondary branch bifurcates from the primary branch via a supercritical pitchfork bifurcation at $d_1 \approx 0.74$ as d_1 decreases. This stable branch represents a family of (localized) unimodal stationary solutions as shown in Fig. 2(a). The bifurcation diagram presented in Fig. 3 suggests that (1.1) with (1.2) has no limit cycles as shown in Fig. 2(b) and (c). This type of bifurcation diagram can be obtained for $\xi \gtrsim 0.67$.

Fig. 4 shows the bifurcation diagram for $\xi = 0.64$. As seen in Fig. 3,

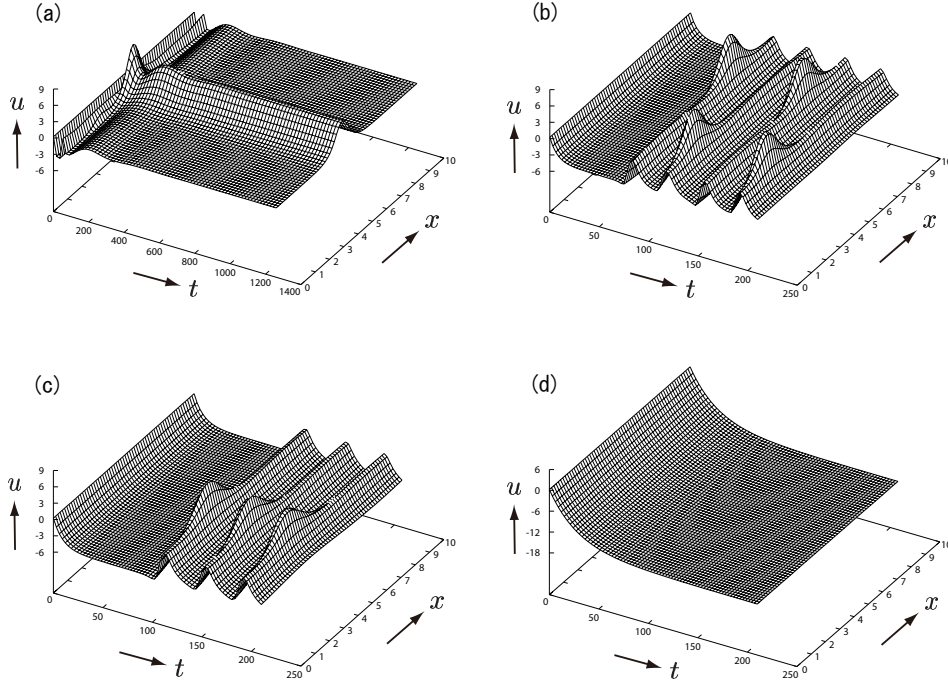


Figure 2: Spatiotemporal patterns appear after some time passes from the initial time for some values of d_1 when $\xi = 0.6$. The initial value is given by $(\xi/2, \xi/2)$ with a small random perturbation. The values of $u(x, t)$ on $(x, t) \in [0, 10] \times [0, 1400]$ or $(x, t) \in [0, 10] \times [0, 250]$ are represented by a 3D graph. The profile of $v(x, t)$ is omitted here because the amplitude and spatial variation of $v(x, t)$ for each t are relatively small compared to those of $u(x, t)$. The numerical solution on $0 \leq x \leq 10$ presented in this figure can be regarded as that on $-5 \leq x \leq 5$ under the periodic boundary condition. (a) $d_1 = 0.1$, A localized unimodal stationary pattern; (b) $d_1 = 0.25$, An oscillatory pattern which exhibits an alternating repetition of spatially homogeneous patterns and localized unimodal patterns with two different positions of their peak. The distance between two peak positions is (almost) $K/2 = 5.0$. (c) $d_1 = 0.4$, An oscillatory pattern which exhibits an alternating repetition of spatially homogeneous patterns and localized unimodal patterns with unique position of their peak. It should be noted that we cannot predict the position of the peak of these localized unimodal patterns in (a)–(c) because of a small random perturbation to the initial value. (d) $d_1 = 0.8$, A spatially homogeneous stationary pattern.

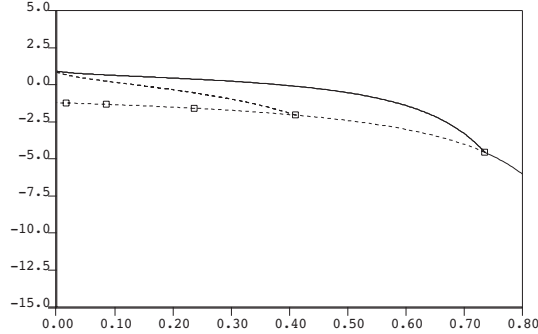


Figure 3: Bifurcation diagram for $\xi = 1.0$. The horizontal and vertical axes indicate d_1 and the size of the u -component of solutions represented by $\frac{1}{K} \int_I u(x) dx$, respectively. The solid line indicates stable solutions, whereas the dashed line indicates unstable ones. The white square indicates the pitchfork bifurcation point. Unstable branches bifurcating from unstable branches for $d_1 \leq 0.30$ are omitted. Notice that the two branches bifurcating from a pitchfork bifurcation point are piled up and are displayed in this bifurcation diagram.

the secondary branch consisting of (localized) unimodal stationary solutions bifurcates from the primary branch consisting of spatially homogeneous equilibria via a supercritical pitchfork bifurcation at $d_1 \approx 0.74$ as d_1 decreases. However, (localized) unimodal stationary solutions on the second branch are unstable for $0.21 \lesssim d_1 \lesssim 0.46$. In fact, the third branch consisting of stable limit cycles as shown in Fig. 2(c) bifurcates from the secondary branch via Hopf bifurcations at $d_1 \approx 0.46$ and $d_1 \approx 0.21$. In this case, we cannot observe limit cycles as shown in Fig. 2(b). This type of bifurcation diagram can be obtained for $0.61 \lesssim \xi \lesssim 0.66$.

Fig. 5 shows the bifurcation diagram for $\xi = 0.60$. As seen in Fig. 4, the third branch consisting of limit cycles as shown in Fig. 2(c) bifurcates from the second branch consisting of (localized) unimodal stationary solutions via Hopf bifurcations at $d_1 \approx 0.53$ and $d_1 \approx 0.14$. However, the third branch

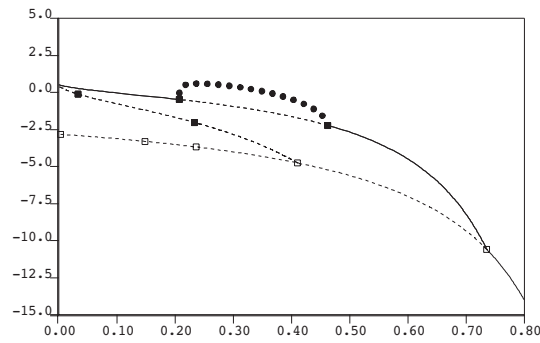


Figure 4: Bifurcation diagram for $\xi = 0.64$. The horizontal and vertical axes indicate d_1 and the size of the u -component of solutions represented by $\frac{1}{K} \max_{t>0} \int_I u(x, t) dx$, respectively. The solid line indicates stable solutions, whereas the dashed line indicates unstable ones. The white and black squares indicate the pitchfork and Hopf bifurcation points, respectively. The curve represented by a family of the black circles \bullet indicates the stable branch of periodic solutions. Unstable branches bifurcating from unstable branches for $d_1 \leq 0.30$ are omitted. Notice that the two branches bifurcating from a pitchfork bifurcation point are piled up and are displayed in this bifurcation diagram.

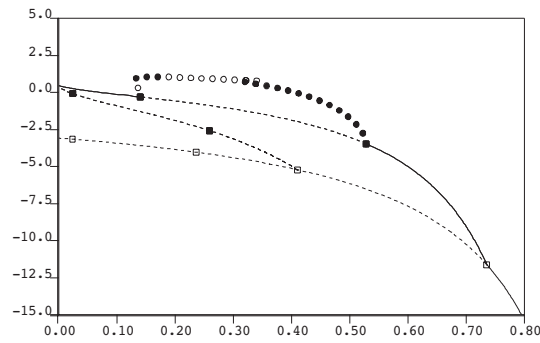


Figure 5: Bifurcation diagram for $\xi = 0.60$. The horizontal and vertical axes indicate d_1 and the size of the u -component of solutions represented by $\frac{1}{K} \max_{t>0} \int_I u(x, t) dx$, respectively. The solid line indicates stable solutions, whereas the dashed line indicates unstable ones. The white and black squares indicate the pitchfork and Hopf bifurcation points, respectively. The curve represented by a family of the black circles \bullet indicates the stable branch of periodic solutions, whereas that of the white circles \circ indicates the unstable ones. Unstable branches bifurcating from unstable branches for $d_1 \leq 0.30$ are omitted. Notice that the two branches bifurcating from a pitchfork bifurcation point are piled up and are displayed in this bifurcation diagram.

has unstable limit cycles for $0.13 \lesssim d_1 \lesssim 0.14$ and $0.18 \lesssim d_1 \lesssim 0.31$. We can observe limit cycles as shown in Fig. 2(b) for $0.18 \lesssim d_1 \lesssim 0.31$, and expect that the fourth branch consisting of these limit cycles bifurcates from the third branch at $d_1 \approx 0.18$ and $d_1 \approx 0.31$ via a period doubling bifurcation. In fact, AUTO indicates a Floquet multiplier passing the unit circle $|\lambda| = 1$ through $\lambda = -1$ around $d_1 \approx 0.18$ and $d_1 \approx 0.31$. At present, it is technically difficult to trace this fourth branch by using AUTO. We can obtain similar bifurcation diagram as in Fig. 5 for $\xi \lesssim 0.60$.

Finally, we note that similar bifurcation structures as above can be obtained near the specific parameter set (2.13). For example, Fig. 6 shows how the bifurcation diagram for $\xi = 0.60$ changes when we change one of the parameter values a_1 , a_2 and d_2 given by (2.13). Thus, we consider that the bifurcation structures presented in this section are structurally stable.

4 Dynamics of spatiotemporal patterns of perturbed system

In this section, we investigate the dynamics of spatiotemporal patterns in the perturbed system (1.3) with (1.2) and (1.4). Our results are useful for understanding the effect of extracellular signaling on cell polarization.

4.1 Motion of localized unimodal pattern

In the same way as subsection 2.2, we find that solutions of (1.3) starting from a spatially homogeneous initial state with small disturbance quickly and temporally approach $(\bar{u}(x - c), \bar{v}(x - c))$ for some $c \in [-K/2, K/2]$ under certain conditions, where \bar{u} and \bar{v} are given by (2.6) and (2.7), respectively. Then, the solutions translationally move to the maximum point of $a_E(x)$ as seen in Fig. 7. We derive the equation of motion for this translational move-

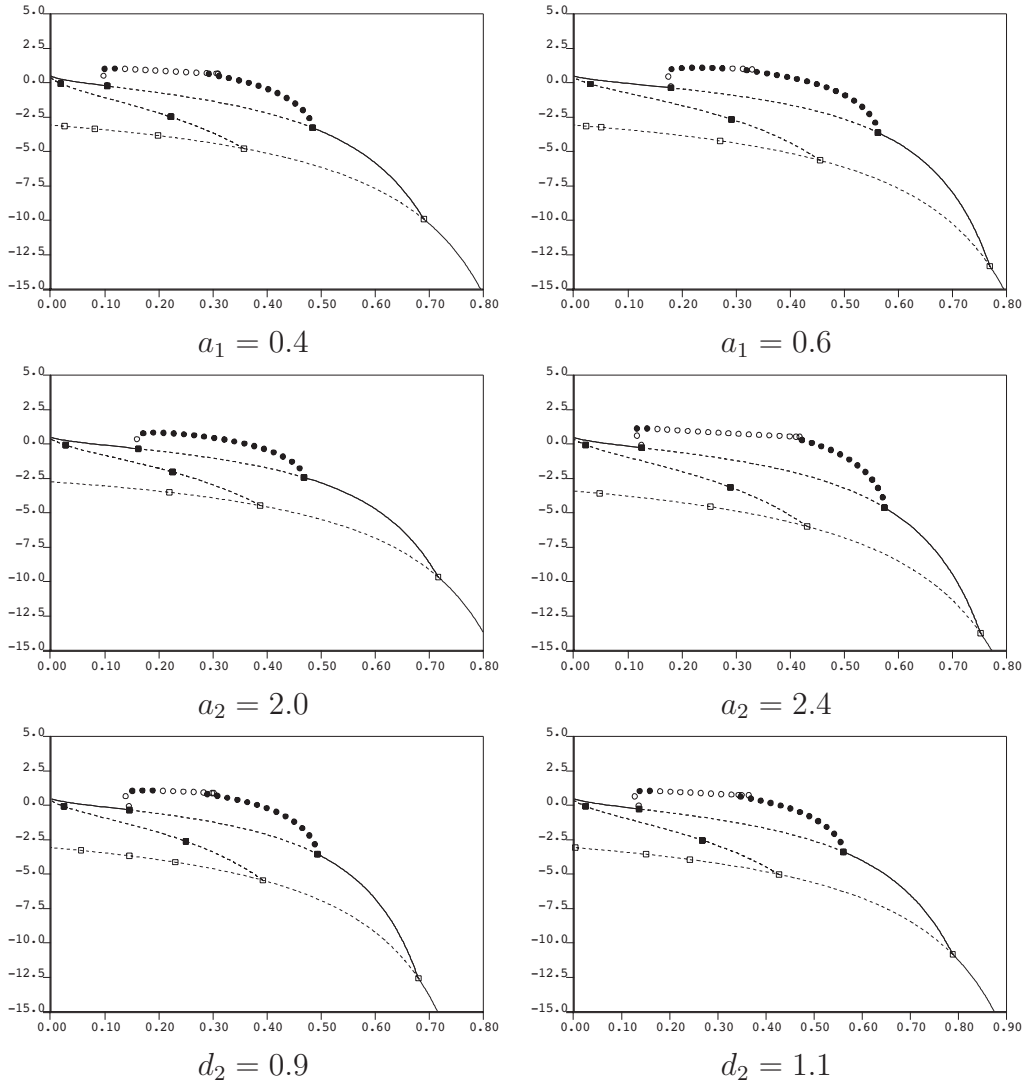


Figure 6: Bifurcation diagrams for $\xi = 0.60$. These bifurcation diagrams are presented in the same way as Fig. 5. The other parameter values except for the indicated value at the bottom of each figure are the same as those used in the bifurcation diagram presented in Fig. 5.

ment according to the theory [9]. To obtain a concrete and exact expression of the equation of motion, we consider

$$a_E(x) = A \cos(2\pi x/K), \quad (4.1)$$

which takes its maximum at $x = 0$.

Let us consider a solution which is well approximated by $S(x - \ell(t))$, where

$$S(x) := (\bar{u}(x), \bar{v}(x)) = (\varphi_1(x), \varphi_2(x)) + O(e^{-bK}). \quad (4.2)$$

In what follows, we derive the equation for $\ell(t)$. From (4.2), we have

$$S_x(x) = w(x)(d_2, -d_1),$$

where

$$w(x) = -\frac{2bp_0}{d_2 - d_1} \operatorname{sech}^2(bx) \tanh(bx) + O(e^{-bK}) \quad (4.3)$$

with

$$b = \frac{1}{2} \sqrt{\frac{(d_2 - d_1)a_1a_2}{d_1d_2}} \quad \text{and} \quad p_0 = \frac{bK}{2} \xi \quad (4.4)$$

by (2.5) and (2.11). Therefore, we see that $w(x) < 0$ for $x > 0$ as mentioned in [9, Lemma 3.2].

Since $f_v(u, v) = -2a_1(u + v)(\alpha u + v) - a_1(u + v)^2 + a_1a_2$ by (1.2), noting (2.8), (2.9) and $p_0q_0 = 3a_2/2$ by the first equation of (2.5), we have

$$\begin{aligned} h_2(x) &:= -\frac{f_v(\bar{u}(x), \bar{v}(x))w(x)}{d_2} \\ &= \frac{2bp_0}{d_2(d_2 - d_1)} \operatorname{sech}^2(bx) \tanh(bx) F(x) + O(e^{-bK}) \end{aligned}$$

where $F(x) := -3a_1a_2 \operatorname{sech}^2(bx) - a_1p_0^2 \operatorname{sech}^4(bx) + a_1a_2$. Let $t = \operatorname{sech}^2(bx)$. Then, we have $F(x) = g(t)$, where

$$g(t) := -3a_1a_2t - a_1p_0^2t^2 + a_1a_2.$$

We see that $F(x)$ is monotone increasing in x for $x > 0$ because $t = \operatorname{sech}^2(bx)$ is monotone decreasing in x for $x > 0$ and $g(t)$ is monotone decreasing in t for $t > 0$. Moreover, $F(0) = g(1) = -2a_1a_2 - a_1p_0^2 < 0$ and $F(K/2) = g(0) + O(e^{-bK}) = a_1a_2 + O(e^{-bK}) > 0$. Therefore, there exists $\beta \in (0, K/2)$ such that $h_2(x) < 0$ for $0 < x < \beta$ and $h_2(x) > 0$ for $\beta < x < K/2$. Furthermore, noting (2.11), a direct calculation with the aid of computer algebra (Mathematica ver.9) shows

$$\begin{aligned} \int_0^{K/2} x h_2(x) dx &= \frac{2ba_1p_0}{d_2(d_2 - d_1)} \left\{ -3a_2 \int_0^\infty x \operatorname{sech}^4(bx) \tanh(bx) dx \right. \\ &\quad \left. - p_0^2 \int_0^\infty x \operatorname{sech}^6(bx) \tanh(bx) dx + a_2 \int_0^\infty x \operatorname{sech}^2(bx) \tanh(bx) dx \right\} \\ &\quad + O(Ke^{-bK}) \\ &= \frac{2ba_1p_0}{d_2(d_2 - d_1)} \left\{ -3a_2 \cdot \frac{1}{6b^2} - p_0^2 \cdot \frac{4}{45b^2} + a_2 \cdot \frac{1}{2b^2} \right\} + O(Ke^{-bK}) \\ &= -\frac{8a_1p_0^3}{45(d_2 - d_1)d_2b} + O(Ke^{-bK}) = -\frac{4a_1p_0^2K\xi}{45(d_2 - d_1)d_2} + O(Ke^{-bK}). \end{aligned}$$

Therefore,

$$\int_0^{K/2} x h_2(x) dx < 0$$

holds if

$$\xi = \frac{1}{K} \int_I (u(x, 0) + v(x, 0)) dx > 0.$$

Hence, we see that the condition (ii) of [9, Proposition 3.6] holds.

Similarly, noting

$$(\operatorname{sech}^2(bx))' = -2b \operatorname{sech}^2(bx) \tanh(bx), \quad \tanh(bx)' = b \operatorname{sech}^2(bx)$$

and $(\varphi_2^*)'' = h_2$, a rather lengthy calculation using the integration by parts

twice shows

$$\begin{aligned} \langle S_z, \Phi^* \rangle &:= -2d_2 \int_0^{K/2} w^2(z) dz + 2(d_2 - d_1) \int_0^{K/2} w(z) \varphi_2^*(z) dz \\ &= -\frac{4p_0^2}{15(d_2 - d_1)} \left\{ \frac{4bd_2}{d_2 - d_1} + \frac{a_1 a_2}{bd_2} + \frac{8a_1 p_0^2}{bd_2} \left(\frac{1}{7} - \frac{1}{3Kb} \right) \right\} + O(Ke^{-bK}) < 0. \end{aligned}$$

Moreover, noting (2.8), (4.1), (4.3) and

$$\cos\left(\frac{2\pi(z + \ell)}{K}\right) - \cos\left(\frac{2\pi(z - \ell)}{K}\right) = -2 \sin\left(\frac{2\pi z}{K}\right) \sin\left(\frac{2\pi \ell}{K}\right),$$

a direct calculation shows

$$\begin{aligned} J(\ell) &:= - \int_0^{K/2} a_1(\bar{u}(z) + \bar{v}(z)) w(z) \{a_E(z + \ell) - a_E(z - \ell)\} dz \\ &= -\frac{4a_1 b p_0^2 A}{d_2 - d_1} \sin\left(\frac{2\pi \ell}{K}\right) \int_0^\infty \operatorname{sech}^4(bz) \tanh(bz) \sin\left(\frac{2\pi z}{K}\right) dz + O(Ke^{-bK}) \\ &= -\frac{4a_1 b p_0^2 A}{d_2 - d_1} \cdot \frac{\pi^3(b^2 K^2 + \pi^2)}{3b^5 K^4} \cdot \operatorname{cosech}\left(\frac{\pi^2}{bK}\right) \sin\left(\frac{2\pi \ell}{K}\right) + O(Ke^{-bK}). \end{aligned}$$

Thus, noting (2.11), it follows from [9, Equation (4.3)] that

$$\frac{d\ell}{dt} = -\varepsilon \left(C \sin\left(\frac{2\pi \ell}{K}\right) + O(Ke^{-bK}) \right) + O(\varepsilon^2), \quad (4.5)$$

where C is given by

$$C = \frac{5a_1 d_2 \pi^3 (b^2 K^2 + \pi^2) A \operatorname{cosech}\left(\frac{\pi^2}{bK}\right)}{b^3 K^4 \left\{ \frac{4b^2 d_2^2}{d_2 - d_1} + a_1 a_2 + \frac{2a_1 b K \xi^2}{21} (3bK - 7) \right\}}$$

with the first equation of (4.4). For example, the value of C is given by $C \approx 6.35 \times 10^{-3}$ under the same condition in the simulation by [15], i.e., $K = 10.0$, $\xi = 2.0$, $d_1 = 0.1$, $A = 1.1$ and the parameter values given by (2.13).

We now examine the validity of (4.5) from a viewpoint of numerical simulations. In a similar manner to the previous section, we numerically solve (1.3) with $a_E(x) = A \cos(\frac{2\pi}{K}(x - \frac{K}{2}))$ on $0 \leq x \leq K$ under the periodic boundary condition. In this case, neglecting error terms, (4.5) is replaced by

$$\frac{d\ell}{dt} = -\varepsilon C \sin\left(\frac{2\pi}{K}\left(\ell - \frac{K}{2}\right)\right). \quad (4.6)$$

Fig. 7 shows that a localized unimodal pattern moves to the maximal point of $a_E(x)$ following the equation of motion given by (4.6). Here, the values of parameters are given by (2.13) and $K = 10.0$, $\xi = 2.0$, $d_1 = 0.1$, $A = 1.1$ and $\varepsilon = 0.1$. The initial value is given by $(\bar{u}(x - c), \bar{v}(x - c))$ with $c = 1.6$, where \bar{u} and \bar{v} are given by (2.6) and (2.7), respectively. Moreover, these results are valid for $0 < \varepsilon \lesssim 0.1$. This suggests that the translational movement of cell polarity can be controlled by sufficiently weak extracellular signals.

Remark 4.1 [15] studied (1.3) by setting $a_2 \rightarrow a_2 \left(1 + \frac{\varepsilon}{2} \sin(\frac{2\pi x}{K})\right)$ in (1.2), which is equivalent to $a_E(x) = A \cos(\frac{2\pi}{K}(x + \frac{K}{4}))$ with $A = a_2/2$.

4.2 Dynamics of spatiotemporal oscillatory patterns

The result in the last subsection suggests that the position of the peak of the final localized unimodal stationary pattern of (1.3) can be determined by the maximum point of $a_E(x)$. In this subsection, we investigate whether or not the perturbed system (1.3) has spatiotemporal oscillatory patterns as seen in Fig. 2 (b) and (c) under the same condition imposed on the unperturbed system (1.1). In particular, we examine whether or not the position of the peak of such unimodal patterns periodically appearing can be determined by the maximum point of $a_E(x)$.

As was mentioned in the last subsection, we numerically solve (1.3) with $a_E(x) = A \cos(\frac{2\pi}{K}(x - \frac{K}{2}))$ on $0 \leq x \leq K$ under the periodic boundary

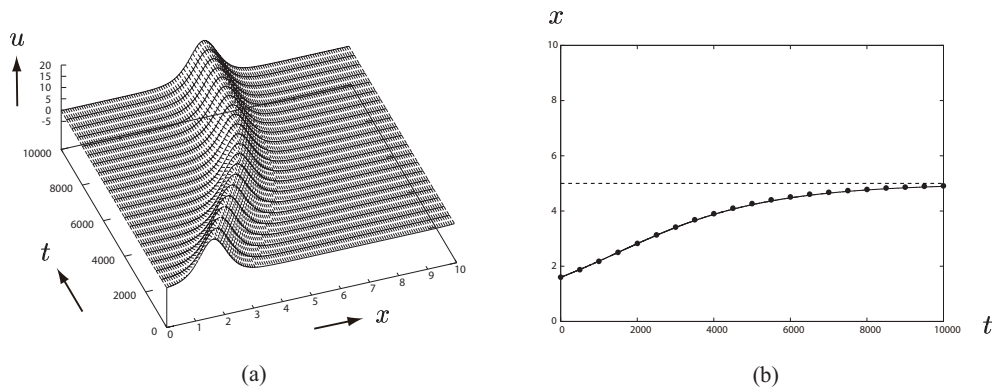


Figure 7: The motion of a localized unimodal pattern in the perturbed system (1.3). The initial value is given by $(\bar{u}(x - c), \bar{v}(x - c))$ with $c = 1.6$, where \bar{u} and \bar{v} are given by (2.6) and (2.7), respectively. (a) The dynamics of u -component. The values of $u(x, t)$ on $0 \leq x \leq 10$ and $0 \leq t \leq 10000$ are represented by a 3D graph. The profile of $v(x, t)$ is omitted here because the amplitude and spatial variation of $v(x, t)$ for each t are relatively small compared to those of $u(x, t)$. (b) The comparison of theory and numerical simulations. The rigid and dashed lines represent a solution of (4.6) with initial value $\ell(0) = 1.6$ and its limit given by $\ell = 5.0$, respectively. The dots represent the maximal point of $u(x, t)$ for $t = 500n$ ($n \in \mathbf{Z}, 0 \leq n \leq 20$).

condition. In the same way as subsection 2.3, we numerically solve (1.3) for $d_1 = 0.1, 0.25, 0.4$ and $d_1 = 0.8$ when $\xi = 0.6$ under the parameter values (2.13) and $K = 10.0, A = 1.1$ and $\varepsilon = 0.1$.

Fig. 8 shows that the perturbed system (1.3) exhibits similar spatiotemporal patterns as seen in Fig. 2. In contrast to the case of the unperturbed system (1.1), the position of the peak of the localized unimodal patterns of the perturbed system (1.3) is determined by the maximum point of $a_E(x)$; i.e., it does not depend on a small random perturbation to initial values. Moreover, it should be noted that the stable limit cycles in the perturbed system (1.3) earlier appear and their period is shorter as compared to those in the unperturbed system (1.1).

When $d_1 = 0.4$, we can observe oscillatory spatiotemporal patterns as presented in Fig. 8 (b) for $0 < \varepsilon \leq 0.1$. In contrast, when $d_1 = 0.25$, we cannot always observe oscillatory spatiotemporal patterns as presented in Fig. 8 (c) for $0 < \varepsilon \leq 0.1$. More precisely, we can observe them for $0.015 \lesssim \varepsilon \leq 0.1$, i.e., the position of the peak of the localized unimodal patterns cannot be determined by the maximum point of $a_E(x)$ for $0 < \varepsilon \lesssim 0.014$. These results suggest that cell polarity oscillations can be controlled by sufficiently weak extracellular signals if the reversal of polarity does not occur.

5 Concluding remarks

It is well recognized that reaction-diffusion models are useful for studying cell polarity formation, as shown in a survey paper [6, 17]. We investigate the oscillatory dynamics and bifurcation structure of a reaction-diffusion model for cell polarity formation in [15]. We show that this model can represent formation processes from a homogeneous initial cell to a polarized cell; the

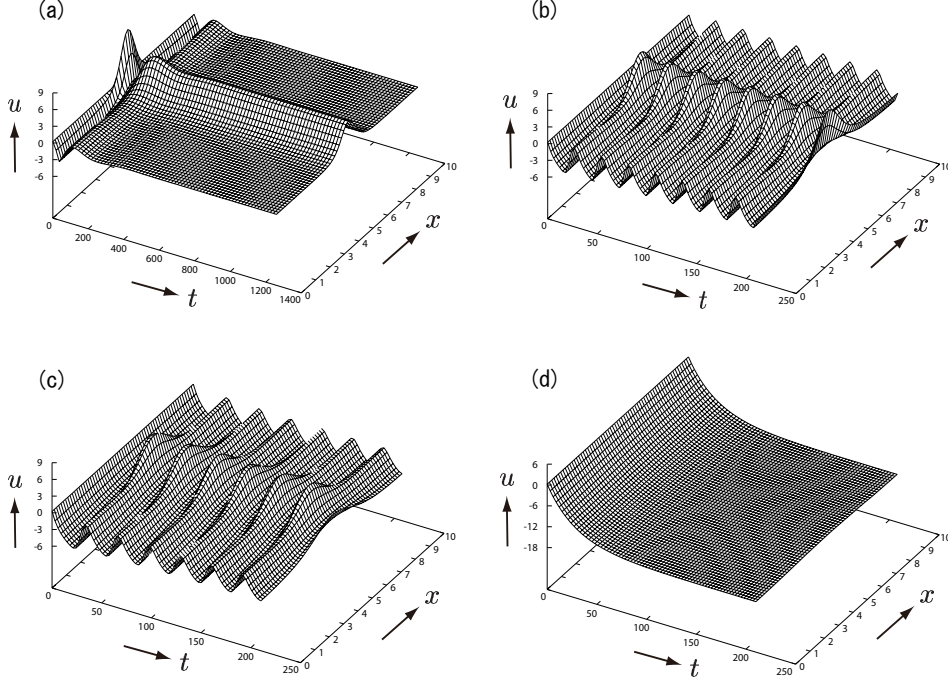


Figure 8: Spatiotemporal patterns appear after some time passes from the initial time for some values of d_1 when $\xi = 0.6$. The initial value is given by $(\xi/2, \xi/2)$ with a small random perturbation. The values of $u(x, t)$ on $(x, t) \in [0, 10] \times [0, 1400]$ or $(x, t) \in [0, 10] \times [0, 250]$ are represented by a 3D graph. The profile of $v(x, t)$ is omitted here because the amplitude and spatial variation of $v(x, t)$ for each t are relatively small compared to those of $u(x, t)$. The numerical solution on $0 \leq x \leq 10$ presented in this figure can be regarded as that on $-5 \leq x \leq 5$ under the periodic boundary condition. (a) A localized unimodal stationary pattern for $d_1 = 0.1$; (b), (c) An oscillatory pattern which exhibits an alternating repetition of spatially homogeneous patterns and localized unimodal patterns with unique position of their peak. The values of d_1 are given by $d_1 = 0.25$ and $d_1 = 0.4$, respectively. In contrast to the case of Fig. 2, it should be noted that the position of the peak of these localized unimodal patterns in (a)–(c) is determined by the maximum point of $a_E(x)$ without depending on a small random perturbation to the initial value. (d) A spatially homogeneous stationary pattern for $d_1 = 0.8$.

polarized cells can be classified into three types including the type of cell polarity oscillations. In particular, it is shown that the Turing instability can be a trigger which eventually leads to cell polarity oscillations with the reversal of polarity. These results suggest that the spatial average and diffusion of two internal chemicals in a cell can provide a similar switching mechanism for cell polarity as shown in [4, 16, 19] based on molecular networks. Moreover, we investigate the effect of extracellular signaling on cell polarity oscillations. Our results suggest that cell polarity oscillations can be controlled by sufficiently weak extracellular signals if the reversal of polarity does not occur.

In simple terms, mathematical models for studying cell polarity oscillations are classified into two types, ODE models and reaction-diffusion models. ODE models are based on detailed molecular networks proper to cells currently being observed, and often have complicated mathematical expressions which are difficult to apply standard mathematical analysis. Moreover, they explicitly or implicitly assume the existence of the front and back of a cell, and hence they cannot represent formation processes from an initially homogeneous cell to a polarized cell. In contrast, although it may be difficult to give an explicit correspondence between reaction-diffusion models and the molecular networks of cells, they can represent formation processes from an initially homogeneous cell to a polarized cell. Moreover, they can clarify universal aspects of cell polarity through standard mathematical analysis if their reaction terms are mathematically simple and biologically reasonable. Therefore, the mutually complementary approaches of ODE models based on molecular networks and reaction-diffusion models for studying macroscopic spatiotemporal dynamics is indispensable for understanding the whole picture of cell polarity oscillations.

Acknowledgments. The first, second, and third authors were supported in part by the JSPS KAKENHI 16K05273, 17K14237, 19H01805, respectively.

References

- [1] J. L. Chern, Y. Morita, and T. T. Shieh, Asymptotic behavior of equilibrium states of reaction-diffusion systems with mass conservation, *J. Diff. Eqns.* **264** (2018), 550–574.
- [2] E. J. Doedel, B. E. Oldeman, A. R. Champneys, F. Dercole, T. Fairgrieve, Y. A. Kuznetsov, R. C. Paffenroth, B. Sandstede, X. Wang, C. Zhang, AUTO-07p: continuation and bifurcation software for ordinary differential equations (2012).
- [3] S. Doerr, K. Ragkousi, Cell polarity oscillations in mitotic epithelia, *Current Opinion in Genetics and Development*, **57** (2019), 47-53.
- [4] M. Guzzo, S. M. Murray, E. Martineau, S. Lhospice, G. Baronian, L. My, et al. A gated relaxation oscillator mediated by FrzX controls morphogenetic movements in *Myxococcus xanthus*, *Nature Microbiology*, **3** (2018), 948-959.
- [5] S. Ishihara, M. Otsuji, A. Mochizuki, Transient and steady state of mass-conserved reaction-diffusion systems, *Phys. Rev. E* **75** (2007), 015203.
- [6] A. Jilkine, L. Edelstein-Keshet, A comparison of mathematical models for polarization of single eukaryotic cells in response to guided cues, *PLoS Comput. Biol.*, **3** (2011), e1001121.

- [7] S. Jimbo, Y. Morita, Lyapunov function and spectrum comparison for a reaction-diffusion system with mass conservation, *J. Diff. Eqns* **255** (2013) 1657-1683.
- [8] M. Kuwamura and H. Izuhara, Diffusion-driven destabilization of spatially homogeneous limit cycles in reaction-diffusion systems, *Chaos*. **27** (2017), 033112.
- [9] M. Kuwamura, S.-S. Lee, S.-I. Ei, Dynamics of localized unimodal patterns in reaction-diffusion systems for cell polarization by extracellular signaling, *SIAM J. Appl. Math.* **78** (2018), 3238-3257.
- [10] M. Kuwamura, Y. Morita, Perturbations and dynamics of reaction-diffusion systems with mass conservation, *Phys. Rev. E* **92** (2015), 012908.
- [11] Y. Liu, W.-C. Lo, Analysis of spontaneous emergence of cell polarity with delayed negative feedback, *Math. Biosci. Eng.* **16** (2019) 1392-1413.
- [12] Y. Mori, A. Jilkine, L. Edelstein-Keshet, Asymptotic and bifurcation analysis of wave-pinning in a reaction-diffusion model for cell polarization, *SIAM J. Appl. Math* **71** (2011) 1401-1427.
- [13] Y. Morita, T. Ogawa, Stability and bifurcation of nonconstant solutions to a reaction-diffusion system with conservation of mass, *Nonlinearity* **23** (2010) 1387-1411.
- [14] T. Okuda Sakamoto, Hopf bifurcation in a reaction-diffusion system with conservation of mass, *Nonlinearity* **26** (2013) 2027-2049.

- [15] M. Otsuji, S. Ishihara, C. Co, K. Kaibuchi, A. Mochizuki, S. Kuroda, A mass conserved reaction-diffusion system captures properties of cell polarity, *PLoS Comp. Biol.* **3** (2007) e108.
- [16] J. Parka, W. R. Holmes, S. H. Lee, H.-N. Kim, D.-H. Kim, M. K. Kwak, C. J. Wang, L. Edelstein-Keshet, A. Levchenko, Mechanochemical feedback underlies coexistence of qualitatively distinct cell polarity patterns within diverse cell populations, *Proc Natl Acad Sci U S A* **114** (2017), E5750-E5759.
- [17] W. J. Rappel, L. Edelstein-Keshet, Mechanisms of cell polarization, *Curr. Opin. Syst. Biol.* **3** (2017), 43–53.
- [18] O. Sliusarenko, J. Neu, D. R. Zusman, G. Oster, Accordion waves in *Myxococcus xanthus*, *Proc Natl Acad Sci U S A* **103** (2006), 1534-1539.
- [19] F. Tostevin, M. Wigbers, L. Søggaard-Andersen, U. Gerland, Four different mechanisms for switching cell polarity, *PLoS Comp. Biol.* **17** (2021) e1008587.